Classification for the universal scaling of Néel temperature and staggered magnetization density of three-dimensional dimerized spin-$\frac{1}{2}$ antiferromagnets

D.-R. Tan, C.-D. Li, and F.-J. Jiang*

Department of Physics, National Taiwan Normal University, 88, Sec. 4, Ting-Chou Rd., Taipei 116, Taiwan

(Received 22 November 2017; published 2 March 2018)

Inspired by the recent theoretical development relevant to the experimental data of $TlCuCl_3$, particularly those associated with the universal scaling between the Néel temperature T_N and the staggered magnetization density M_s, we carry out a detailed investigation of three-dimensional (3D) dimerized quantum antiferromagnets using the first-principles quantum Monte Carlo calculations. Through this study we wish to better understand the microscopic effects on these scaling relations of T_N and M_s, hence to shed light on some of the observed inconsistency between the theoretical and the experimental results. Remarkably, for the considered 3D dimerized models, we find that the established universal scaling relations are not only valid, but can each be categorized within its kind by the amount of stronger antiferromagnetic couplings connected to each spin. Convincing numerical evidence is provided to support the validity of this classification scheme. Based on all the related results known in the literature, we further argue that the proposed categorization for the universal scaling investigated in our paper should be applicable for 3D dimerized spin systems with (certain kinds of) quenched disorder and (or) on lattice geometries other than those considered here. The relevance of the outcomes presented in this investigation to the experiments of $TlCuCl_3$ is briefly discussed as well.

DOI: 10.1103/PhysRevB.97.094405

I. INTRODUCTION

While, in general, certain intriguing properties related to the phase transitions of classical models are governed by the thermal fluctuations, many interesting characteristics of different phases of quantum systems are triggered by quantum fluctuations at zero temperature [1–5]. In other words, a great deal of attractive phenomena of quantum systems are observed at the low temperature regions where quantum fluctuations play the dominated roles in determining the properties of these systems. Still, for quantum systems, thermal fluctuations and the interplay between the effects from finite temperatures and zero temperatures may lead to compelling and fascinating results. Two noticeable examples are the quantum critical regime (QCR) associated with two-dimensional (2D) antiferromagnets, and the universal scaling between the Néel temperature T_N and the staggered magnetization density M_s of three-dimensional (3D) quantum spin systems.

Theoretically, QCR is characterized by the appearance of several finite-temperature universal behaviors among some physical quantities of the underlying 2D spin systems [6–8]. On one hand, based on the relevant analytic calculations, for the dimerized Heisenberg model, this regime should exist at any parametric value associated with spatial anisotropy. On the other hand, several numerical studies imply that the exotic characteristics of QCR can only be confirmed rigorously at the finite temperature regions above the related quantum critical points (QCPs), where a dramatic change in the ground states occurs due to very strong quantum fluctuations [9–14]. In other words, the QCR serves as a classical case in which close connections between two categories of properties of a system may exist, despite the fact that they seem to be unrelated to each other at a first glance.

Another remarkable illustration of surprising connections between the thermal and the ground-state properties of a quantum system is the 3D dimerized spin-1/2 Heisenberg models, which will be investigated in detail here.

Recently, the experimental results of $TlCuCl_3$ have stimulated several theoretical investigations [15–25]. In particular, the phase diagram of $TlCuCl_3$ under pressure motivates a few analytic and numerical explorations of three universal scalings between a thermal and a ground state property of 3D dimerized quantum antiferromagnets. For example, it is demonstrated that for three different 3D dimerized spin-1/2 Heisenberg models, the data collapse of the physical quantity $T_N/T^\star$ as functions of M_s leads to a universal curve [19]. In other words, for these three various dimerized systems, when the data of $T_N/T^\star$ are treated as functions of M_s, they fall on top of a smooth curve. Here T_N is the Néel temperature, $T^\star$ is the temperature where the observable uniform susceptibility χ_u reaches its maximum value, and M_s is the staggered magnetization density. Similar smooth scaling appears as well if the quantity $T_N/\overline{J}$ is considered instead of $T_N/\overline{J}$ [19]. Here $\overline{J}$ is the summation of the antiferromagnetic coupling strength connected to each spin of any of the studied dimerized models. Later it is shown that these scaling relations emerge for disordered systems as well [26,27].

Although the agreement between the data of $TlCuCl_3$ and the related analytic and numerical results is impressive, some controversial observations need to be clarified. For instance, while theoretically the appearance of smooth curves resulting from data collapse seems to support the scenario that generic scaling relations between T_N and M_s

*fjjiang@ntnu.edu.tw

do exist, experimental data indicate these universal relations may depend on the microscopic details of the investigated models [15,16,21].

To uncover whether there indeed are generic scaling relations between T_N and M_s for 3D dimerized spin-1/2 antiferromagnets, in this paper we conduct a large-scale quantum Monte Carlo (QMC) calculation for several 3D spatially anisotropic spin-1/2 Heisenberg models. It is interesting to note the models studied in Ref. [19] that lead to universal data collapse have the following property: specifically, among the antiferromagnetic bonds connected to any spin, only one bond is of stronger coupling strength. Inspired by this observation, the considered 3D dimerized systems in this paper can be classified by the amount of strong bonds linked to each spin.

As anticipated, based on our numerical results, we find the established universal scaling relations mentioned above do appear for the models considered here. While the emergence of such scaling relations is foreseen, it is remarkable, and unexpected as well, that the data collapse using the related physical quantities of the models having the same amount of strong bonds emerged from any spin form their own smooth universal curves. In particular, the (universal) curves of the models with different numbers of strong bonds attached to every spin differ from one another. In other words, for the studied models, any one of the considered universal scalings can be individually categorized by the amount of strong bonds connected to each spin. Later we will argue that this classification for the universal scaling of T_N and M_s of 3D dimerized spin models should be applicable even for systems with (certain kinds of) quenched disorder and (or) on lattice geometries other than those considered here.

The detailed investigation presented in this paper not only reinforces the robustness of the known universal scaling between T_N and M_s for 3D dimerized quantum antiferromagnets, but also takes these relations further by establishing quantitatively their classification. We would like to emaphsize the fact that the outcomes shown here are useful for related experiments as well. For example, by comparing the theoretical predictions and the associated data, one can propose the most applicable model for the targeted material. Moreover, this model can then be considered to explore some further theoretical properties of that material.

The rest of this paper is organized as follows. After the introduction, the studied 3D dimerized spin-1/2 models and the measured observables are briefly described. Then the obtained numerical data and the resulting analysis outcomes are summarized. In particular, the evidence to support the validity of the classification for the considered universal scaling relations outlined above is discussed in detail. Finally, a section is devoted to conclude the investigation presented here.

II. MICROSCOPIC MODELS AND OBSERVABLES

The 3D dimerized quantum Heisenberg models investigated here are given by the Hamilton operators

$$H_1 = \sum_{\langle ij\rangle} J_{ij}\,\vec{S}_i\cdot\vec{S}_j + \sum_{\langle i'j'\rangle} J'_{i'j'}\,\vec{S}_{i'}\cdot\vec{S}_{j'}, \tag{1}$$

$$H_2 = \sum_i J_\perp \vec{S}_{i,1}\cdot\vec{S}_{i,2} + \sum_{\langle ij\rangle,\alpha=1,2} J_{ij,\alpha}\,\vec{S}_{i,\alpha}\cdot\vec{S}_{j,\alpha} + \sum_{\langle i'j'\rangle,\alpha=1,2} J'_{i'j',\alpha}\,\vec{S}_{i',\alpha}\cdot\vec{S}_{j',\alpha}, \tag{2}$$

where, in Eq. (1), J_{ij} and $J'_{i'j'}$ are the antiferromagnetic couplings (bonds) connecting nearest neighbor spins $\langle ij\rangle$ and $\langle i'j'\rangle$ located at a 3D cubical lattice, respectively, and $\vec{S}_i$ is the spin-1/2 operator at site i. Notice the α in the second equation, which takes the value of either 1 or 2, stands for the indices of the considered two copies of 3D cubical lattices. In addition, the $J_\perp$ appearing above are the couplings connecting spins that belong to different copies of the two targeted 3D cubical lattices. Finally, the other parameters and the operators showing up in Eq. (2) have the same definitions as their counterparts without the subscript α in Eq. (1). It should be pointed out that, in this paper, we have set $J_{ij} = J_{ij,1} = J_{ij,2} = J = 1.0$ and $J'_{i'j'} = J'_{i',j',1} = J'_{i'j',2} = J_\perp = J'$ with $J' > J = 1.0$ for any $\langle ij\rangle$ and $\langle i'j'\rangle$. Figure 1 demonstrates the four dimerized spin-1/2 models studied here. Notice for the models of the top (bottom) two panels in Fig. 1, among the bonds touching each spin, three (two) of them have larger magnitude in antiferromagnetic strength than of the others. For convenience, in this investigation the models in Fig. 1 will be called 3D cubical model (top left), double-cube-plaquette model (top right), double-cube-ladder model (bottom left), and 3D plaquette model (bottom right), respectively. Finally, since the couplings J' and J satisfy $J' > J$, each of the investigated systems will undergo a quantum phase transition when the corresponding ratio J'/J exceeds a particular value.

To determine the Néel temperature T_N, the staggered magnetization density M_s, as well as $T^\star$ of the considered

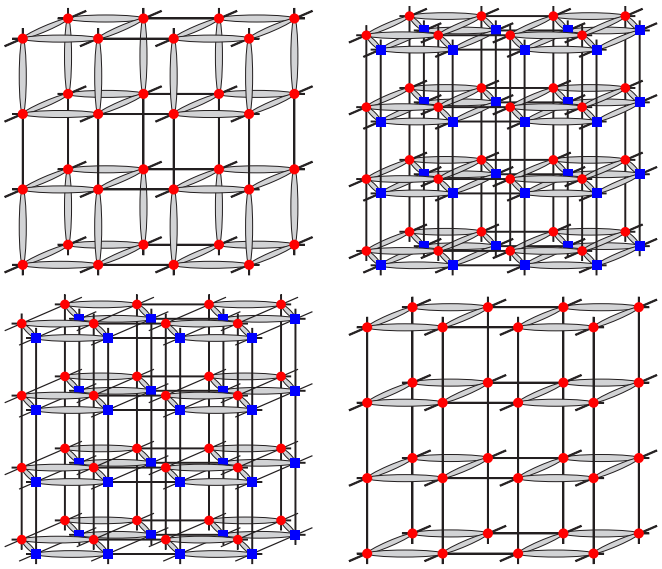

FIG. 1. The 3D dimerized spin-1/2 Heisenberg models investigated in this study: 3D cubical model (top left), double-cube-plaquette model (top right), double-cube-ladder model (bottom left), and 3D plaquette model (bottom right). Notice the antiferromagnetic coupling strength for the thick bonds and thin bonds are given by J' and J, respectively.

dimerized models, the observable staggered structure factor $S(\pi,\pi,L_1,L_2,L_3)$ on a finite lattice with linear sizes L_1, L_2, and L_3 are measured. In addition, both the spatial and temporal winding numbers squared ($\langle W_i^2\rangle$ for $i \in \{1,2,3\}$ and $\langle W_t^2\rangle$), spin stiffness ρ_s, first Binder ratio Q_1, and second Binder ratio Q_2 are calculated in our simulations as well. The quantity $S(\pi,\pi,L_1,L_2,L_3)$ takes the form

$$S(\pi,\pi,L_1,L_2,L_3) = 3\left\langle \left(m_s^z\right)^2\right\rangle, \tag{3}$$

where $m_s^z = \frac{1}{L_1L_2L_3}\sum_i (-1)^{i_1+i_2+i_3} S_i^z$ with S_i^z being the third component of the spin-1/2 operator $\vec{S}_i$ at site i. Moreover, the spin stiffness ρ_s has the following expression:

$$\rho_s = \frac{1}{3}\sum_{i=1,2,3}\rho_{si} = \frac{1}{3\beta}\sum_{i=1,2,3}\frac{\langle W_i^2\rangle}{L_i}, \tag{4}$$

where β is the inverse temperature. Finally the observables Q_1 and Q_2 are defined by

$$Q_1 = \frac{\left\langle \left|m_s^z\right|\right\rangle^2}{\left\langle \left(m_s^z\right)^2\right\rangle} \tag{5}$$

and

$$Q_2 = \frac{\left\langle \left(m_s^z\right)^2\right\rangle^2}{\left\langle \left(m_s^z\right)^4\right\rangle}, \tag{6}$$

respectively. With these observables, the physical quantities required for our paper, namely T_N, M_s, and $T^\star$, can be calculated accurately.

III. THE NUMERICAL RESULTS

To understand the robustness of the scaling relations associated with T_N and M_s, namely to uncover the rules of under what conditions the data collapse employing results from different models will lead to the same universal curves, we have carried out a large-scale QMC simulation using the stochastic series expansion (SSE) algorithm with a very efficient loop-operator update [28]. Before presenting the numerical outcomes obtained from the QMC simulations, it should be pointed out that, in our calculations related to the double-cube-plaquette model (double-cube-ladder model), due to the spatial arrangement of its antiferromagnetic bonds, the linear box sizes (size) L_1 and

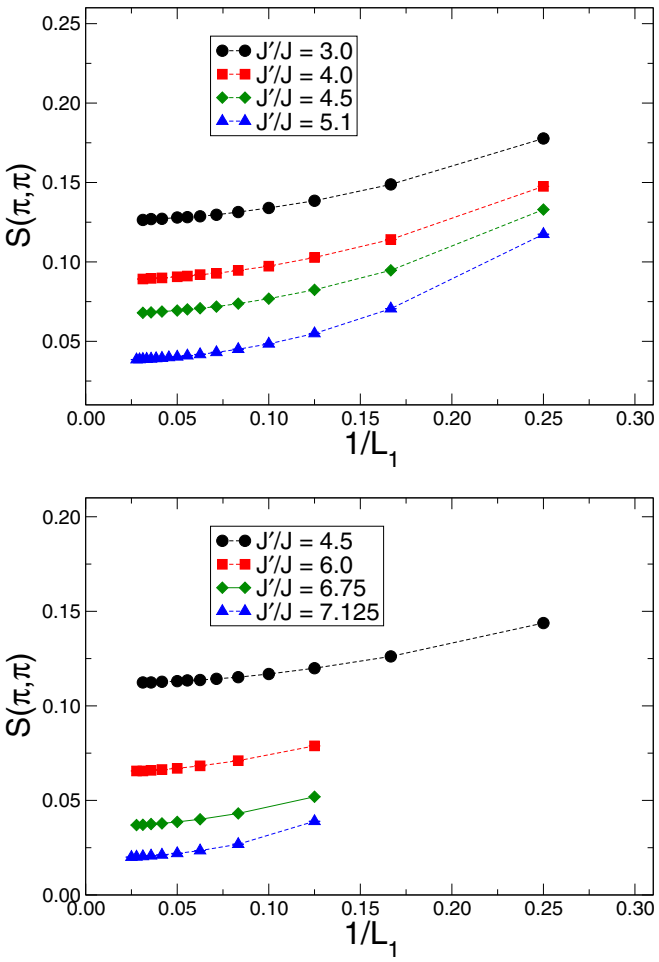

FIG. 2. The $1/L_1$ dependence of the staggered structure factors $S(\pi,\pi)$ for several considered J'/J of the 3D cubical model (top panel) and the double-cube-plaquette model (bottom panel). The dashed lines are added to guide the eye.

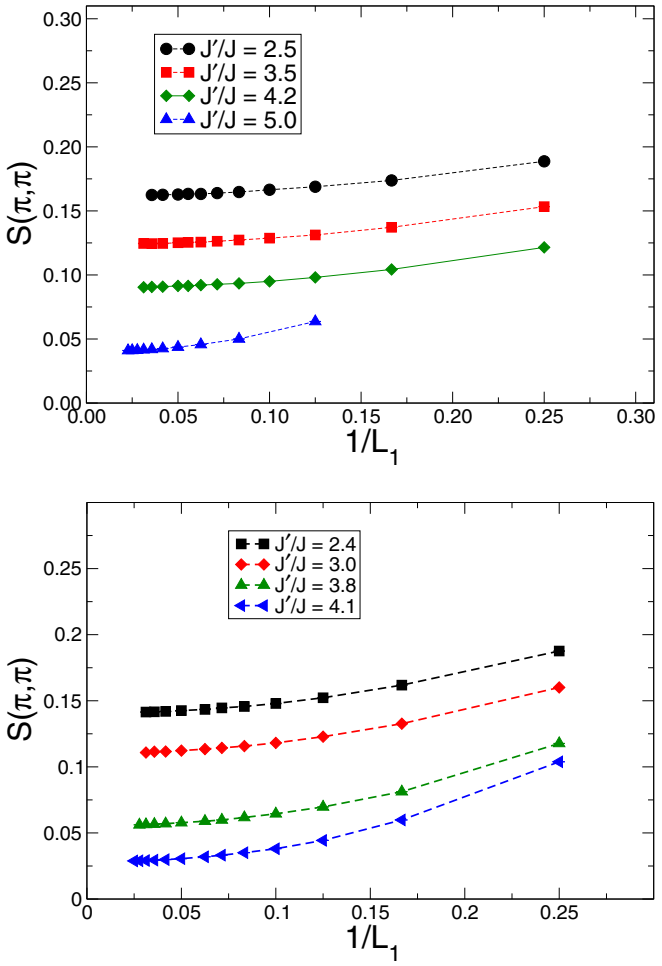

FIG. 3. The $1/L_1$ dependence of the staggered structure factors $S(\pi,\pi)$ for several considered J'/J of the double-cube-ladder model (top panel) and the 3D plaquette model (bottom panel). The dashed lines are added to guide the eye.

L_2 (L_1) used in the simulations are twice that of L_3 (those of L_2 and L_3) for most of the considered J'/J ($J'/J \geqslant 4.4$) [29]. This strategy guarantees the aspect ratios among the three spatial winding numbers squared are kept within certain range. Consequently, the 3D features of these models are preserved. For the 3D cubical model and the 3D plaquette model, the condition $L_1 = L_2 = L_3$ is used in the related calculations.

In the following, we will first detail the determination of M_s.

A. The determination of M_s

The observable considered for the calculations of M_s is $S(\pi,\pi)(L_1)$ [30]. Specifically, for a given J'/J, the associated M_s is given by $\sqrt{S(\pi,\pi)(L_1 \to \infty)}$. We would like to point out that to determine M_s using this approach, the zero temperature, namely the ground state values of $S(\pi,\pi)(L_1)$, are required. Therefore, the simulations related to the calculations of M_s are conducted using the condition $\beta = 2L_1$ [31]. For each of the considered models, we have additionally carried out several simulations (for some selected J'/J) with $\beta = 4L_1$. The results obtained from these trial calculations agree very well with those determined by employing the relation $\beta = 2L_1$ in the simulations.

For each of the studied models, the corresponding $1/L_1$-dependence of the ground state $S(\pi,\pi)$ for some considered J'/J is depicted in Figs. 2 and 3. Motivated by the theoretical predictions in Ref. [32], the determination of M_s is done by extrapolating the staggered structure factors at finite box sizes to their bulk results, using the following three *Ansätze*:

$$a_0 + a_2/L_1^2, \tag{7}$$

$$b_0 + b_2/L_1^2 + b_3/L_1^3, \tag{8}$$

$$c_0 + c_2/L_1^2 + c_3/L_1^3 + c_4/L_1^4. \tag{9}$$

For each good fit ($\chi^2/\mathrm{DOF} \leqslant 2.0$), the corresponding bulk M_s is calculated by $M_s = \sqrt{F}$ with $F = a_0, b_0$, or c_0, depending on which *Ansatz* is used for the fit. The numerical values of M_s determined from the fits employing *Ansätze* Eqs. (7)–(9) for all four models are shown in Figs. 4 and 5. The agreement between the results of M_s determined from different *Ansätze* is remarkably good, and the ones obtained with *Ansatz* Eq. (8) are used in the following analysis.

We would like to emphasize the fact that since three spatial dimensions is the upper critical dimension of the quantum phase transitions investigated in this paper, when approaching

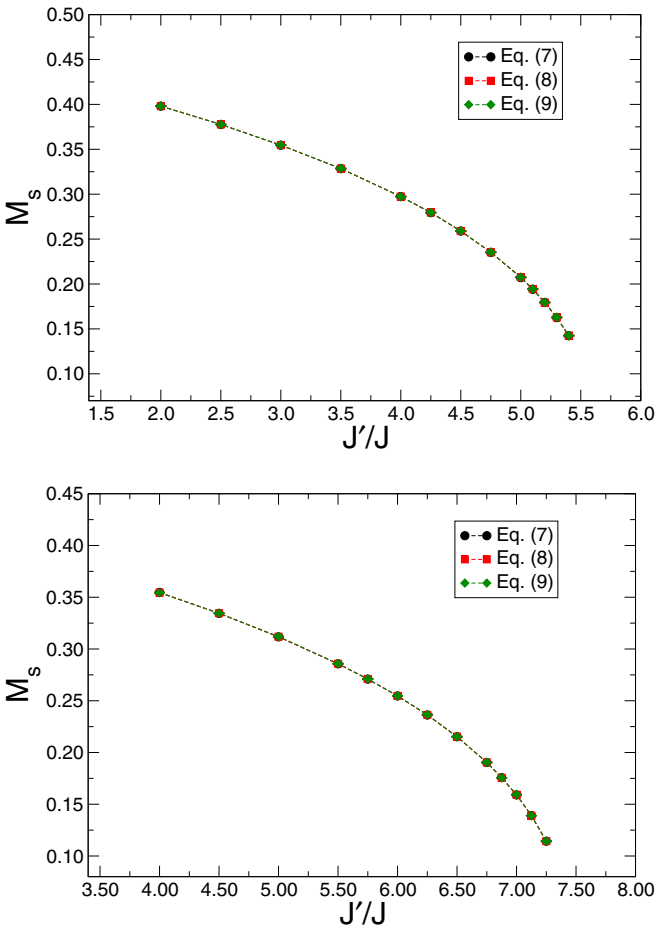

FIG. 4. M_s as functions of the considered J'/J for the 3D cubical model (top panel) and the double-cube-plaquette model (bottom panel). The dashed lines are added to guide the eye.

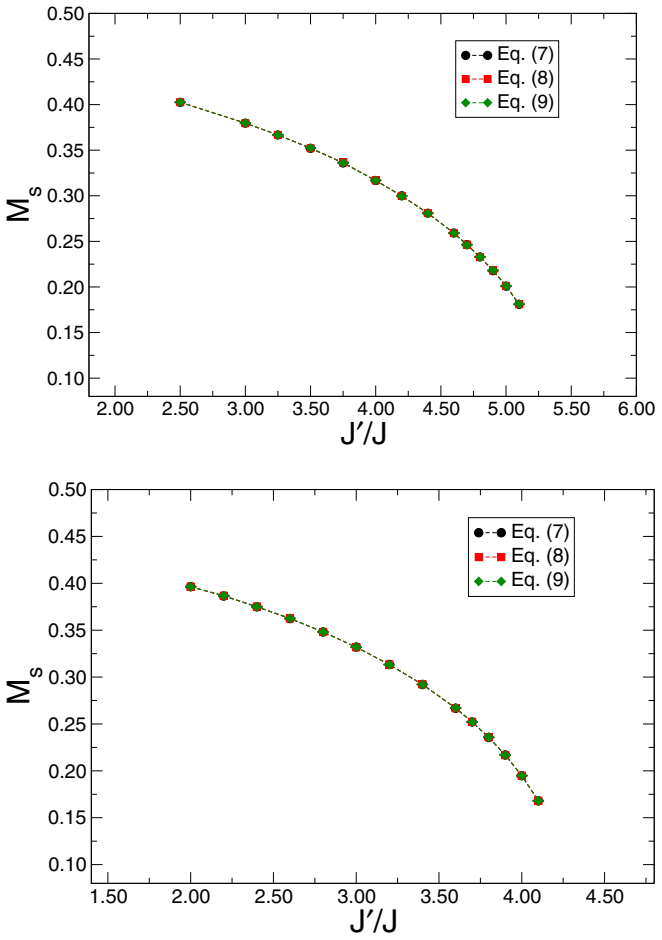

FIG. 5. M_s as functions of the considered J'/J for the double-cube-ladder model (top panel) and the 3D plaquette model (bottom panel). The dashed lines are added to guide the eye.

the critical points, one expects to observe logarithmic corrections to M_s (and T_N as well). The theoretical calculations of the critical exponents associated with these logarithmic corrections are available in Refs. [22,33,34], and the predicted values are confirmed by careful analyses of M_s and T_N/J conducted in Refs. [22,27]. To perform an analysis associated with the mentioned logarithmic corrections requires data of M_s close to the related QCPs. Besides, the motivation of the investigation presented here is to understand to what extent the considered scaling relations are universal. Therefore, a detailed exploration of the logarithmic corrections related to the investigated phase transitions will be left for a future project.

B. The determination of T_N

The Néel temperatures T_N for various J'/J of the four studied models are calculated from the observables $\rho_s L$ [which is given by $(\sum_{i=1}^{3} \rho_{si} L_i)/3$], Q_1, as well as Q_2. Notice bootstrap-type fits using a constrained standard finite-size scaling *Ansatz* of the form $(1 + b_0 L^{-\omega})(b_1 + b_2 t L^{1/\nu} + b_3 (t L^{1/\nu})^2 + ...)$, up to second, third, and (or) fourth order in $t L^{1/\nu}$ are performed in the determination of T_N. Here b_i for $i = 0, 1, 2, ...$ are some constants and $t = \frac{T - T_N}{T_N}$. For some J'/J, *Ansatz* up to fifth order in $t L^{1/\nu}$ is used. The data of $\rho_s L$, Q_1, and Q_2 of some considered J'/J for the investigated models are shown in Figs. 6 and 7.

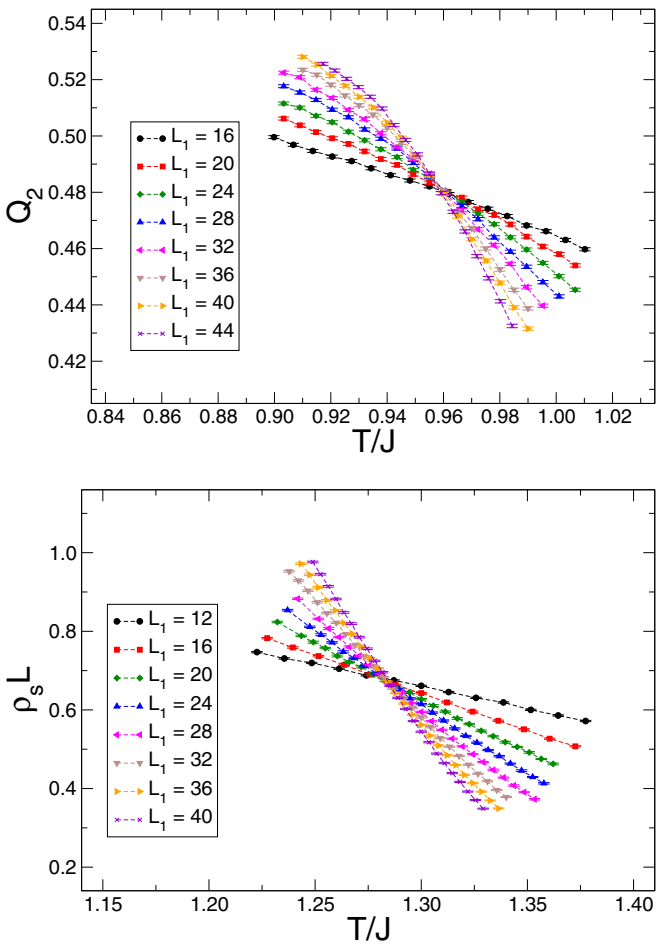

FIG. 6. Top panel: Q_2 of the 3D cubical model as functions of T/J for $J'/J = 5.0$ and $L_1 = 16, 20, 24, 28, 32, 36, 40, 44$. Bottom panel: $\rho_s L$ of the double-cube-plaquette model as functions of T/J for $J'/J = 6.5$ and $L_1 = 12, 16, 20, 24, 28, 32, 36, 40$. The dashed lines are added to guide the eye.

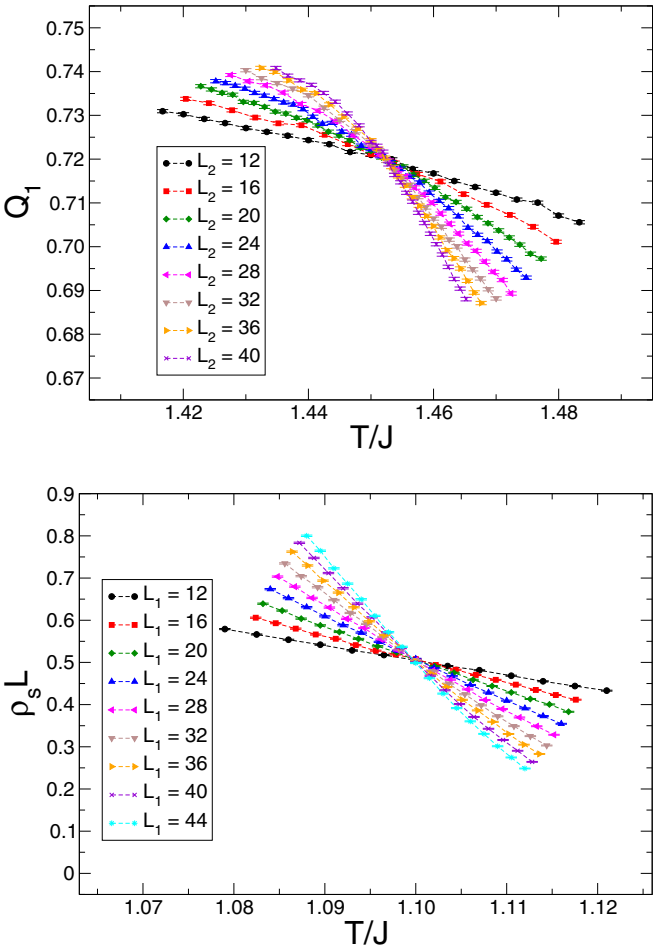

FIG. 7. Top panel: Q_1 of the double-cube-ladder model as functions of T/J for $J'/J = 3.5$ and $L_2 = 12, 16, 20, 24, 28, 32, 36, 40$. Bottom panel: $\rho_s L$ of the 3D plaquette model as functions of T/J for $J'/J = 3.0$ and $L_1 = 12, 16, 20, 24, 28, 32, 36, 40, 44$. The dashed lines are added to guide the eye.

In our analysis related to the calculations of T_N, a fit is treated as a good fit if the corresponding χ^2/DOF satisfies $\chi^2/\text{DOF} \leqslant 2.0$. For few cases, in particular those associated with the observables $\rho_s L$, the criterion for good fits is slightly less restricted ($\chi^2/\text{DOF} \leqslant 2.5$ is used for these situations). For every J'/J of each studied model, fits are carried out with *Ansätze* of various order in $t L^{1/\nu}$. Furthermore, for a given J'/J, several sets of data having different minimum box sizes are considered for the fits as well. The quoted values of T_N in this paper are estimated by averaging the corresponding results of good fits. In addition, the error bar of each cited T_N is estimated conservatively from the uncertainty of every individual T_N of the associated good fits. The determined T_N from the three used observables, namely $\rho_s L$, Q_1, and Q_2 for all the studied models are shown in Fig. 8.

C. The determination of $T^\star$

For all four investigated models, the corresponding $T^\star$, namely the temperatures at which χ_u reach their maximum

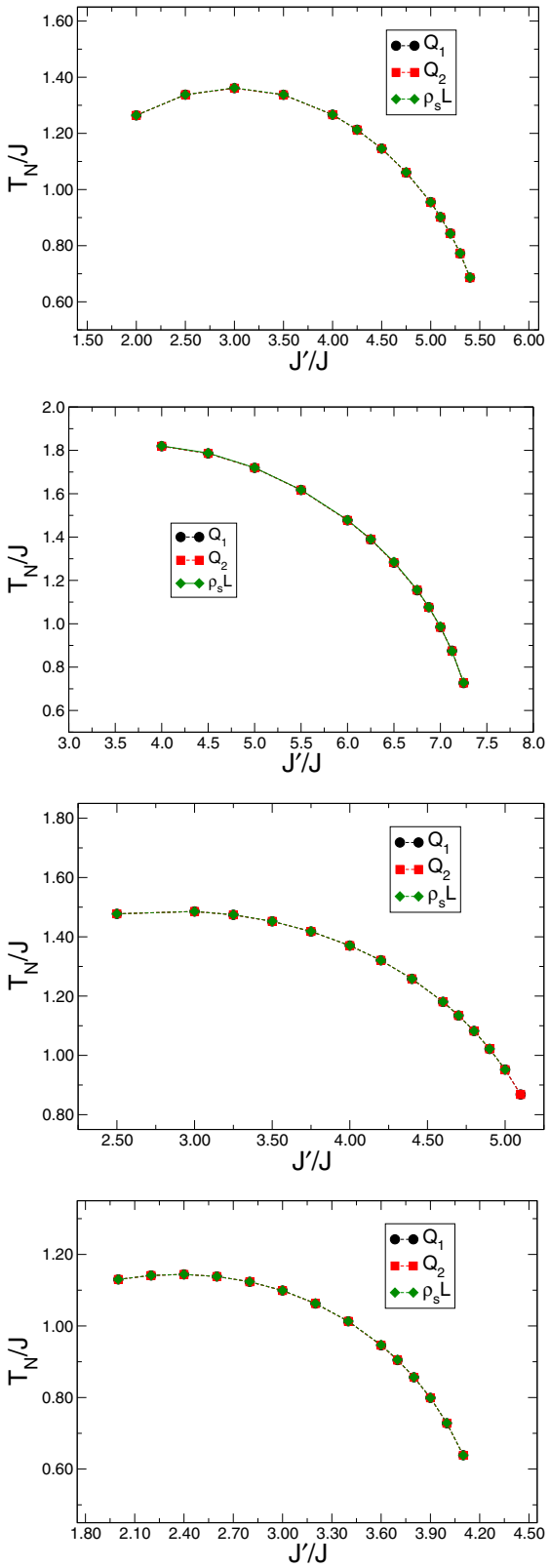

FIG. 8. The J'/J dependence of T_N obtained from Q_1, Q_2, and $\rho_s L$, for the 3D cubical model (top panel), the double-cube-plaquette model (second panel), the double-cube-ladder model (second to last panel), and the 3D plaquette model (bottom panel). Notice the T_N from $\rho_s L$ for $J'/J = 5.1$ of the double-cube-ladder model is not included in the sub-figure.

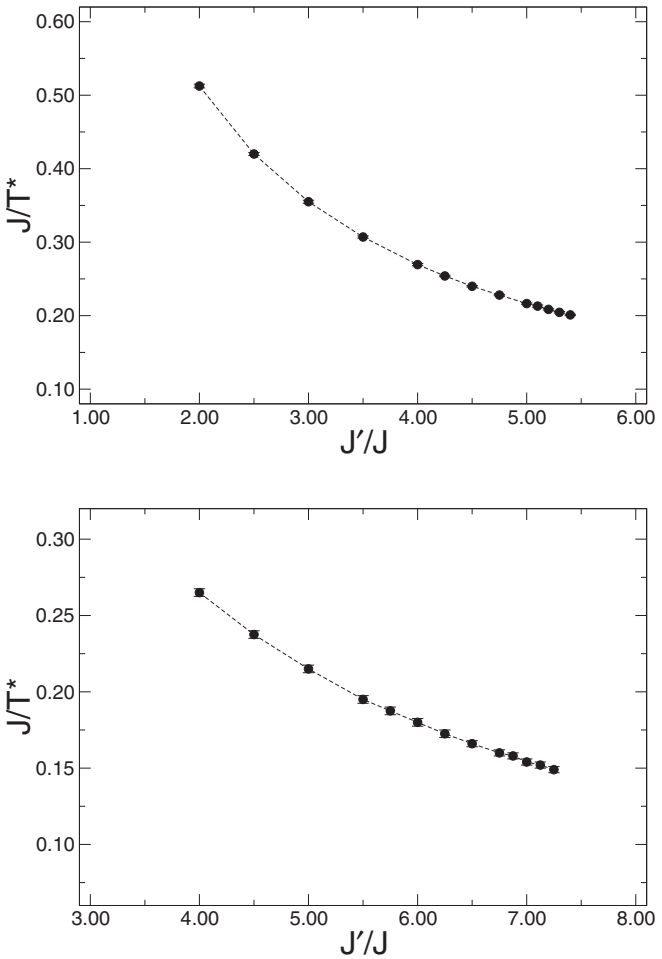

FIG. 9. The inverse of $T^\star$ as functions of J'/J for the 3D cubical model (top panel) and the double-cube-plaquette model (bottom panel).

value, are determined on lattices with moderate large box sizes such as $(L_1, L_2, L_3) = (16,16,16)$, $(24,12,12)$, and so on. The obtained estimations of the inverse of $T^\star$ as functions of J'/J are shown in Figs. 9 and 10. For each individual model, several additional simulations on lattice with larger or smaller box sizes than those associated with the results demonstrated in Figs. 9 and 10 are conducted at some selected values of J'/J. These trial simulations confirm that for these selected J'/J, the corresponding outcomes presented in Figs. 9 and 10 are indeed the bulk results. Therefore the used $T^\star$ in the relevant analysis should be reliable.

D. The scaling relations between $T_N/\overline{J}$, $T_N/T^\star$, and M_s

Having obtained M_s, T_N, and $T^\star$, we now turn to study the scaling relation(s) between $T_N/\overline{J}$ ($T_N/T^\star$) and M_s (M_s). Figure 11 shows T_N/J as functions of M_s for all four considered models. The results in Fig. 11 indicate there are no any universal relations for T_N/J and M_s among the investigated dimerized systems. While no obvious connection is observed among the curves of T_N/J (as functions of M_s) shown in Fig. 11, it is interesting to notice that the deviation from linearity for those curves becomes more transparent when $M_s \geqslant 0.25$. In other words, the nonlinear dependence of T_N/J

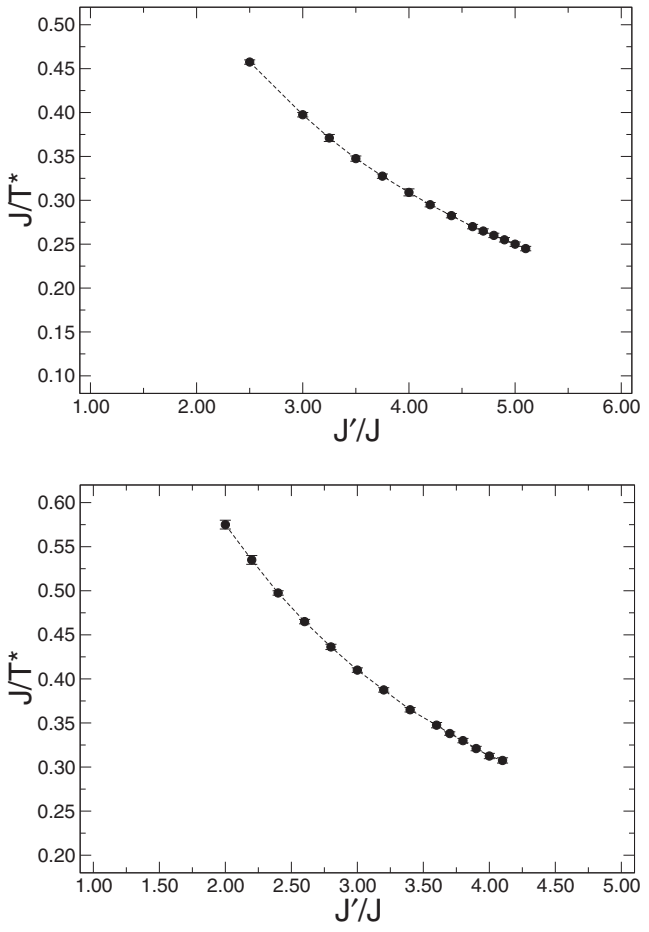

FIG. 10. The inverse of $T^\star$ as functions of J'/J for the double-cube-ladder model (top panel) and the 3D plaquette model (bottom panel).

on M_s begins to appear as the associated data are obtained relatively away from $(J'/J)_c$. This is consistent with the results concluded in Ref. [35].

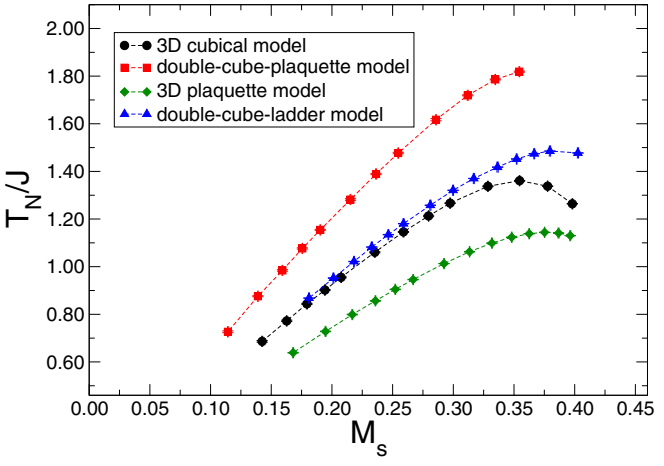

FIG. 11. T_N/J as functions of M_s for all considered 3D dimerized models. The used values of T_N in the figure are from the observable Q_1.

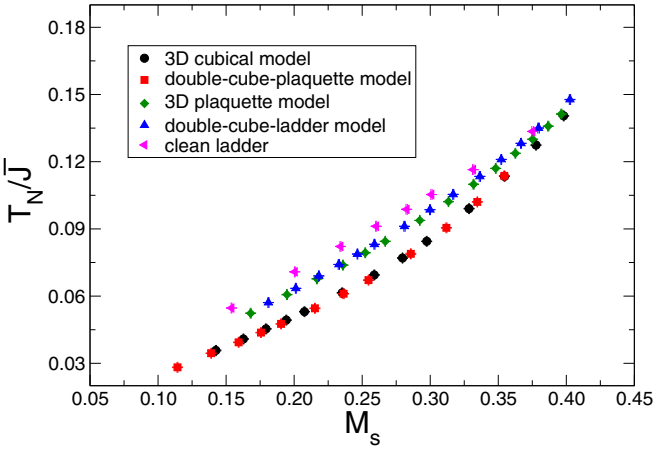

FIG. 12. $T_N/\overline{J}$ as functions of M_s for all considered models in this paper. The used values of T_N in the figure are from the observable Q_1. For comparison purposes, some results of the 3D dimerized ladder model, which has one strong bond emerged from each spin, are included here as well [20].

Remarkably, while no obvious scaling relations are observed when T_N/J are treated as functions of M_s, such universal dependence of T_N on M_s do emerge if the quantities $T_N/\overline{J}$ and $T_N/T^\star$ are considered. This can be clearly seen in Figs. 12 and 13. Specifically, the data of $T_N/\overline{J}$ and $T_N/T^\star$ of these studied models do fall on top of their individual universal curves when these two quantities are regarded as functions of M_s. The most striking result shown in Figs. 12 and 13 is that these universal scaling curves can be categorized by the amount of bonds which are connected to each spin and have stronger antiferromagnetic coupling strength J'. Indeed, from the outcomes demonstrated in these figures, one can see that the universal curves corresponding to the 3D cubical model and the double-cube-plaquette model, which have three bonds of coupling strength J' linked to each spin, are different from those of the 3D plaquette model and the double-cube-ladder model for which there are two bonds of coupling strength J' surrounding

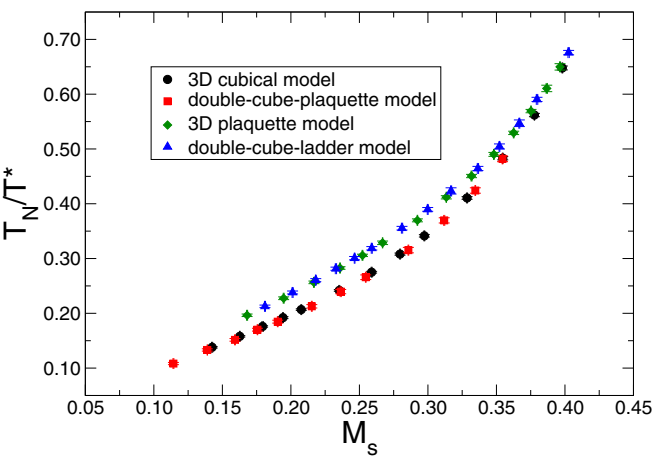

FIG. 13. $T_N/T^\star$ as functions of M_s for all considered models in this paper. The used values of T_N in the figure are from the observable Q_1.

every spin. Notice for comparison purposes, the data of the 3D dimerized spin-1/2 ladder model [20], which has one strong bond emerged from any spin, are included in Fig. 12 as well.

To conclude, Figs. 12 and 13 show convincing evidence that any one of the universal scaling relations investigated here can be categorized within its type by the amount of stronger antiferromagnetic bonds connected to each spin, at least for the models considered in this paper. We will argue later that this classification scheme regarding the studied universal scaling relations should be a generic one.

IV. DISCUSSIONS AND CONCLUSIONS

For certain types of 3D dimerized quantum antiferromagnets, it is demonstrated that universal scaling relations appear when the physical quantities $T_N/\overline{J}$ and $T_N/T^\star$ are considered as functions of M_s [19]. Furthermore, near the associated QCPs, these mentioned observables scale linearly with M_s. Similar phenomena are observed for disordered models as well [26]. Motivated by these findings, in this paper we have investigated four 3D dimerized spin-1/2 Heisenberg models, using the first principles nonperturbative QMC simulations. Notice the models studied in Ref. [19] have the feature that among the bonds connected to any spin there is only one bond with stronger antiferromagnetic coupling strength. According to this observation, for the models considered here and for any of their spin p, either two or three bonds linked to it possess stronger antiferromagnetic coupling strength than of the others touching the same spin p.

Remarkably, universal scaling relations associated with T_N and M_s do emerge for the four models studied here. In particular, among these four dimerized systems, the data collapse of $T_N/\overline{J}$ and $T_N/T^\star$ of the models having the same amount of strong bonds emerged from any spin do form their own smooth universal curves. Furthermore, the curves of the models associated with two strong bonds attached to each spin are different from those of the models possessing three strong bonds coming out from every spin. In other words, the universal scaling considered in this paper can be categorized by the amount of strong bonds connected to each spin. Our findings considerably generalize those established in the literature.

It will be of great interest to understand the classification scheme discovered here from a theoretical perspective. This requires detailed calculations of the relevant field theory and is beyond the scope of our paper. To gain an intuitive explanation of the results found in this paper, one first notices that, as the magnitude of J'/J increases, the resulting curves of $\overline{J}$ of the models with different amounts of strong bonds attached to each spin diverge farther and farther away from each other, while those related to the systems having the same number of J' coupling connected to any of their spins stay close with one another. A similar (and much more satisfactory) scenario is observed for the quantity $T^\star$ as well. These results indicate that, for those J'/J near the associated QCPs, if the corresponding $\overline{J}$ (or $T^\star$) are considered as the relevant energy scales, models with the same amount of strong bonds emerged from each spin have energy scales that take similar numerical values. As a result, close to the considered QCPs, the classification scheme found here is not completely unexpected. It is compelling that the proposed categorization for the universal scaling studied here is valid for a broad range of M_s, even when one is deep inside the antiferromagnetic phase. In summary, to better understand the results reached here, it will be desirable to obtain the relevant analytic expressions for the universal scaling relations investigated in this paper.

It is also interesting to notice the outcomes reached here are consistent with the experimental results of $TlCuCl_3$. Indeed, the data of $TlCuCl_3$ in Refs. [15,16,21] indicate the curves associated with the universal scaling of $T_N/T^\star$ and M_s most likely depend on the microscopic details of the studied systems. This is in agreement with the main result obtained in our investigation.

Finally, we would like to point out that in Ref. [27], it is shown that for both a 3D spin-1/2 antiferromagnet with the so-called configurational disorder and the 3D regular dimerized ladder quantum Heisenberg model, data collapse of $T_N/\overline{J}$ (as functions of M_s) using the results from both systems leads to a smooth universal curve as well. Notice for a model with configurational disorder, each spin has exactly one strong bond connected to it for every disordered realization. Furthermore, while the number of bonds tied to every spin of the double-cube-type models considered here is seven, the other two investigated models have six bonds connected to any of their spins. Based on these observations, it is likely that the results obtained here, i.e., the universal scaling relations of 3D dimerized spin-1/2 antiferromagnets investigated in this paper can be categorized by the amount of strong bonds linked to every spin, are applicable for systems with (certain kinds of) quenched disorder and (or) on lattice geometries other than those considered in this paper. To verify whether this is indeed the case or not, particularly to examine if microscopic details have any impact on these explored scaling relations, besides studying models on the cubic and the double-cubic lattices with different arrangement of spatial anisotropy from the ones employed here [36], simulating 3D antiferromagnets on the honeycomb lattice and other disordered systems will shed light on justifying this conjecture.

ACKNOWLEDGMENT

This paper is partially supported by Ministry of Science and Technology of Taiwan (MOST 105-2112-M-003-002-MY3).

[1] N. Goldenfeld, *Lectures On Phase Transitions And The Renormalization Group*, Frontiers in Physics (Addison-Wesley, Reading, MA, 1992).

[2] L. D. Landau and E. M. Lifshitz, *Statistical Physics*, 3rd ed., Part 1, Course of Theoretical Physics, Vol. 5 (Pergamon Press, Oxford , 1994).

[3] L. D. Carr, *Understanding Quantum Phase Transitions*, Condensed Matter Physics (CRC Press, Boca Raton, FL, 2010).

[4] S. Sachdev, *Quantum Phase Transitions*, 2nd ed. (Cambridge University Press, Cambridge, 2011).

[5] L. E. Reichl, *A Modern Course in Statistical Physics*, 4th ed. (Wiley-VCH, Weinheim, 2016).

[6] A. V. Chubukov and S. Sachdev, Phys. Rev. Lett. **71**, 169 (1993).
[7] A. V. Chubukov and S. Sachdev, Phys. Rev. Lett. **71**, 2680 (1993).
[8] A. V. Chubukov, S. Sachdev, and J. Ye, Phys. Rev. B **49**, 11919 (1994).
[9] A. W. Sandvik, A. V. Chubukov, and S. Sachdev, Phys. Rev. B **51**, 16483 (1995).
[10] M. Troyer, H. Kontani, and K. Ueda, Phys. Rev. Lett. **76**, 3822 (1996).
[11] M. Troyer, Masatoshi Imada, and Kazuo Ueda, J. Phys. Soc. Jpn. **66**, 2957 (1997).
[12] J.-K. Kim and M. Troyer, Phys. Rev. Lett. **80**, 2705 (1998).
[13] Y. J. Kim, R. J. Birgeneau, M. A. Kastner, Y. S. Lee, Y. Endoh, G. Shirane, and K. Yamada, Phys. Rev. B **60**, 3294 (1999).
[14] Y. J. Kim and R. J. Birgeneau, Phys. Rev. B **62**, 6378 (2000).
[15] Ch. Rüegg, N. Cavadini, A. Furrer, H.-U. Güdel, K. Krämer, H. Mutka, A. Wildes, K. Habicht, and P. Vorderwisch, Nature (London) **423**, 62 (2003).
[16] C. Ruegg, B. Normand, M. Matsumoto, A. Furrer, D. F. McMorrow, K. W. Kramer, H. U. Gudel, S. N. Gvasaliya, H. Mutka, and M. Boehm, Phys. Rev. Lett. **100**, 205701 (2008).
[17] Y. Kulik and O. P. Sushkov, Phys. Rev. B **84**, 134418 (2011).
[18] J. Oitmaa, Y. Kulik, and O. P. Sushkov, Phys. Rev. B **85**, 144431 (2012).
[19] S. Jin and A. W. Sandvik, Phys. Rev. B **85**, 020409(R) (2012).
[20] M.-T. Kao and F.-J. Jiang, Eur. Phy. J. B **86**, 419 (2013).
[21] P. Merchant, B. Normand, K. W. Krämer, M. Boehm, D. F. McMorrow, and Ch. Rüegg, Nat. Phys. **10**, 373 (2014).
[22] Yan Qi Qin, Bruce Normand, Anders W. Sandvik, and Z. Y. Meng, Phys. Rev. B **92**, 214401 (2015).
[23] H. Scammell and O. Sushkov, Phys. Rev. B **92**, 220401 (2015).
[24] H. Scammell and O. Sushkov, Phys. Rev. B **95**, 024420 (2017).
[25] H. Scammell and O. Sushkov, Phys. Rev. B **95**, 094410 (2017).
[26] D.-R. Tan and F.-J. Jiang, Eur. Phys. J. B **88**, 289 (2015).
[27] D.-R. Tan and F.-J. Jiang, Phys. Rev. B **95**, 054435 (2017).
[28] A. W. Sandvik, Phys. Rev. B **59**, R14157(R) (1999).
[29] For our calculations of M_s and $T^\star$ associated with the double-cube-plaquette model, all three spatial linear box sizes are equal for the simulations of $J'/J = 4.0$ and 4.5.
[30] Since for a fixed J'/J of every considered model, the three linear box sizes L_1, L_2, and L_3 are either equal or having fixed ratios, the abbreviations $S(\pi,\pi)(L_1)$ and $S(\pi,\pi)$ will be used for $S(\pi,\pi,L_1,L_2,L_3)$ if no confusion may occur.
[31] For the determination of M_s, the values of β used for all the simulations with $L \leqslant 10$ are $\beta J = 24.0$.
[32] J. Cardy, *Scaling and Renormalization in Statistical Physics* (Cambridge University Press, Cambridge, 1996).
[33] R. Kenna, Nucl. Phys. B **691**, 292 (2004).
[34] R. Kenna, in *Order, Disorder and Criticality*, edited by Y. Holovatch (World Scientific, Singapore, 2012), Vol. 3, Chap. 1.
[35] H. D. Scammell, Y. Kharkov, Yan Qi Qin, Zi Yang Meng, B. Normand, and O. P. Sushkov, Phys. Rev. B **96**, 174414 (2017).
[36] After submitting the manuscript, we have simulated another 3D dimerized spin-1/2 Heisenberg model (on the cubic lattice) with the property that there are three strong bonds attached to each of its spins. The preliminary results obtained are consistent with the scenario concluded in this paper.